Hindawi Publishing Corporation
Shock and Vibration
Volume 2016, Article ID 2450573, 13 pages
http://dx.doi.org/10.1155/2016/2450573

Research Article

Study on the Rollover Characteristic of In-Wheel-Motor-Driven Electric Vehicles Considering Road and Electromagnetic Excitation

Di Tan, Haitao Wang, and Qiang Wang

School of Transportation and Vehicle Engineering, Shandong University of Technology, Zibo 255049, China

Correspondence should be addressed to Di Tan; di.tan@mail.scut.edu.cn

Received 4 January 2016; Revised 5 March 2016; Accepted 20 March 2016

Academic Editor: Vadim V. Silberschmidt

For in-wheel-motor-driven electric vehicles, the motor is installed in the wheel directly. Tyre runout and uneven load can cause magnet gap deformation in the motor, which will produce electromagnetic forces that further influence the vehicle rollover characteristics. To study the rollover characteristics, a verified 16-degree-of-freedom rollover dynamic model is introduced. Next, the vehicle rollover characteristics both with and without electromagnetic force are analyzed under conditions of the Fixed Timing Fishhook steering and grade B road excitation. The results show that the electromagnetic force has a certain effect on the load transfer and can reduce the antirollover performance of the vehicle. Therefore, the effect of the electromagnetic force on the rollover characteristic should be considered in the vehicle design. To this end, extensive analysis was conducted on the effect of the road level, vehicle speed, and the road adhesion coefficient on the vehicle rollover stability. The results indicate that vehicle rollover stability worsens when the above-mentioned factors increase, the most influential factor being the road adhesion coefficient followed by vehicle speed and road level. This paper can offer certain theory basis for the design of the in-wheel-motor-driven electric vehicles.

1. Introduction

As one of the most important auto safety problems, vehicle rollover accidents have gained more attention in recent years [1]. Many researchers have conducted significant research on vehicle rollover with a traditional chassis structure [2–4]. However, most of the research is focused on the lateral dynamics and the classic three-degree-of-freedom model is adopted as the basis, without considering the effect of road excitation [5–7]. Taking into account the effect of the road excitation, a seven-degree-of-freedom combined model was developed based on a vehicle with a traditional chassis in [8]. Vehicle rollover was analyzed under certain conditions, and the results indicated that the combined model could reflect the vehicle rollover features more accurately compared with the traditional three-degree-of-freedom model. However, the road input correlation of four wheels was ignored in the study.

For the in-wheel motors (IWMs) electric vehicles (EVs), driving motors are integrated in the wheels directly [9, 10]. The tyre runout under different road surface roughness (RSR) excitations and uneven load will cause deformation in the IWM magnet gap. The magnet gap deformation (MGD) can lead to an unbalanced electromagnetic force (EMF), which will influence the vehicle rollover stability [11]. At present, research on IWM driven systems is still in its infancy. Relatively little research has been conducted on topics such as the EMF excitation caused by the RSR and their combined effect on the vehicle rollover. In this paper, the rollover prediction model of an IWM driven EV without a speed reducer is given, including a verified 16-degree-of-freedom coupling dynamic model with the nonlinear tyre model. Then the mathematical model of the excitation source is established which includes the RSR model that considers the input correlation of four wheels, the IWM EMF model that calculates the EMF, and the steering input model. Based on these models, comparative analysis of the vehicle rollover with or without EMF is carried out under the condition of the Fixed Timing Fishhook (FTF) steering and grade B RSR excitation to understand the influence of EMF on the vehicle rollover. In addition, further analysis is conducted

to understand the effect of road conditions on the vehicle rollover, such as the road level, vehicle speed, and road adhesion coefficient.

2. Rollover Model of IWM Driven EV

2.1. Rollover Prediction Dynamics Model

2.1.1. 16-Degree-of-Freedom Rollover Dynamic Model. A rear IWM driven EV without speed reducer is used for this study. The basic structure of the IWM driven system is shown in Figure 1 [12].

Based on the structure in Figure 1, a dynamic model with 16 degrees of freedom is given, which can reflect the vehicle dynamic characteristics in different directions, as shown in Figure 2. The 16 degrees of freedom include three degrees of freedom for the longitudinal, lateral, and yawing movement of the vehicle, three degrees of freedom for the vertical, pitch, and roll movement of the vehicle body, four degrees of freedom for the rotational movement of the wheels, and six degrees of freedom for the vertical movement of the unsprung mass. In this paper, the model is used to study the rollover characteristics of IWM driven EVs and is termed as a rollover prediction dynamic model.

The dynamic equation of the rollover model shown in Figure 2 is given by

$$
\begin{aligned}
&m\left(\dot{u}-v\gamma+\dot{z}_s\dot{\theta}\right)-m_s h_s\ddot{\theta}-\left(F_{x\mathrm{fl}}+F_{x\mathrm{fr}}\right)\cos\delta+\left(F_{y\mathrm{fl}}\right.\\
&\quad\left.+F_{y\mathrm{fr}}\right)\sin\delta-F_{x\mathrm{rl}}-F_{x\mathrm{rr}}=0,\\
&m\left(\dot{v}+u\gamma-\dot{z}_s\dot{\varphi}\right)+m_s h_s\ddot{\varphi}-\left(F_{x\mathrm{fl}}+F_{x\mathrm{fr}}\right)\sin\delta-\left(F_{y\mathrm{fl}}\right.\\
&\quad\left.+F_{y\mathrm{fr}}\right)\cos\delta-F_{y\mathrm{rl}}-F_{y\mathrm{rr}}=0,\\
&I_z\dot{\gamma}-\left(F_{x\mathrm{fl}}\sin\delta+F_{x\mathrm{fr}}\sin\delta\right)l_{\mathrm{f}}-\left(F_{y\mathrm{fl}}\cos\delta\right.\\
&\quad\left.+F_{y\mathrm{fr}}\cos\delta\right)l_{\mathrm{f}}+\left(F_{y\mathrm{rl}}+F_{y\mathrm{rr}}\right)l_{\mathrm{r}}-\left(F_{y\mathrm{fl}}\sin\delta\right.\\
&\quad\left.-F_{y\mathrm{fr}}\sin\delta\right)\frac{d}{2}-\left(F_{x\mathrm{fr}}\cos\delta-F_{x\mathrm{fl}}\cos\delta+F_{x\mathrm{rr}}\right.\\
&\quad\left.-F_{x\mathrm{rl}}\right)\frac{d}{2}+I_{xz}\ddot{\varphi}=0,\\
&I_x\ddot{\varphi}-m_s g h_s\varphi+m_s h_s a_y+I_{xz}\dot{\gamma}+\frac{d}{2}\left[k_{12}\left(z_1-z_{11}\right)\right.\\
&\quad+c_{12}\left(\dot{z}_1-\dot{z}_{11}\right)+k_{32}\left(z_3-z_{33}\right)+c_{32}\left(\dot{z}_3-\dot{z}_{33}\right)\\
&\quad-k_{22}\left(z_2-z_{21}\right)-c_{22}\left(\dot{z}_2-\dot{z}_{21}\right)-k_{42}\left(z_4-z_{43}\right)\\
&\quad\left.-c_{42}\left(\dot{z}_4-\dot{z}_{43}\right)\right]=0,\\
&I_y\ddot{\theta}+m_s a_x h_s-l_{\mathrm{f}}\left[k_{12}\left(z_1-z_{11}\right)+c_{12}\left(\dot{z}_1-\dot{z}_{11}\right)\right.\\
&\quad\left.+k_{22}\left(z_2-z_{21}\right)+c_{22}\left(\dot{z}_2-\dot{z}_{21}\right)\right]+l_{\mathrm{r}}\left[k_{32}\left(z_3-z_{33}\right)\right.\\
&\quad\left.+c_{32}\left(\dot{z}_3-\dot{z}_{33}\right)+k_{42}\left(z_4-z_{43}\right)+c_{42}\left(\dot{z}_4-\dot{z}_{43}\right)\right]\\
&\quad=0,\\
&m_s\left(\ddot{z}_s+v\dot{\varphi}-u\dot{\theta}\right)+k_{12}\left(z_1-z_{11}\right)+c_{12}\left(\dot{z}_1-\dot{z}_{11}\right)\\
&\quad+k_{22}\left(z_2-z_{21}\right)+c_{22}\left(\dot{z}_2-\dot{z}_{21}\right)+k_{32}\left(z_3-z_{33}\right)\\
&\quad+c_{32}\left(\dot{z}_3-\dot{z}_{33}\right)+k_{42}\left(z_4-z_{43}\right)+c_{42}\left(\dot{z}_4-\dot{z}_{43}\right)=0,\\
&m_{\mathrm{fl1}}\ddot{z}_{11}+k_{11}\left(z_{11}-q_1\right)+c_{11}\left(\dot{z}_{11}-\dot{q}_1\right)+k_{12}\left(z_{11}-z_1\right)\\
&\quad+c_{12}\left(\dot{z}_{11}-\dot{z}_1\right)=0,\\
&m_{\mathrm{fr1}}\ddot{z}_{21}+k_{21}\left(z_{21}-q_2\right)+c_{21}\left(\dot{z}_{21}-\dot{q}_2\right)+k_{22}\left(z_{21}\right.\\
&\quad\left.-z_2\right)+c_{22}\left(\dot{z}_{21}-\dot{z}_2\right)=0,\\
&\left(m_{\mathrm{rl1}}+m_{\mathrm{rl5}}\right)\ddot{z}_{31}+k_{31}\left(z_{31}-q_3\right)+c_{31}\left(\dot{z}_{31}-\dot{q}_3\right)\\
&\quad+k_{33}\left(z_{31}-z_{33}\right)+c_{33}\left(\dot{z}_{31}-\dot{z}_{33}\right)+k_{35}\left(z_{31}-z_{33}\right)\\
&\quad+c_{35}\left(\dot{z}_{31}-\dot{z}_{33}\right)=0,\\
&\left(m_{\mathrm{rl3}}+m_{\mathrm{rl4}}\right)\ddot{z}_{33}+k_{32}\left(z_{33}-z_3\right)+c_{32}\left(\dot{z}_{31}-\dot{z}_3\right)\\
&\quad+k_{33}\left(z_{33}-z_{31}\right)+c_{33}\left(\dot{z}_{33}-\dot{z}_{31}\right)+k_{35}\left(z_{33}-z_{31}\right)\\
&\quad+c_{35}\left(\dot{z}_{33}-\dot{z}_{31}\right)=0,\\
&\left(m_{\mathrm{rr1}}+m_{\mathrm{rr5}}\right)\ddot{z}_{41}+k_{41}\left(z_{41}-q_4\right)+c_{41}\left(\dot{z}_{41}-\dot{q}_4\right)\\
&\quad+k_{43}\left(z_{41}-z_{43}\right)+c_{43}\left(\dot{z}_{41}-\dot{z}_{43}\right)+k_{45}\left(z_{41}-z_{43}\right)\\
&\quad+c_{45}\left(\dot{z}_{41}-\dot{z}_{43}\right)=0,\\
&\left(m_{\mathrm{rr3}}+m_{\mathrm{rr4}}\right)\ddot{z}_{43}+k_{42}\left(z_{43}-z_4\right)+c_{42}\left(\dot{z}_{43}-\dot{z}_4\right)\\
&\quad+k_{43}\left(z_{43}-z_{41}\right)+c_{43}\left(\dot{z}_{43}-\dot{z}_{41}\right)+k_{45}\left(z_{43}-z_{41}\right)\\
&\quad+c_{45}\left(\dot{z}_{43}-\dot{z}_{41}\right)=0,\\
&I_{w_i}\dot{w}_i-T_{mi}+F_{xi}r_t=0.
\end{aligned}
\tag{1}
$$

For the research object in this paper is a rear IWM driven EV, the driving torque of the front wheels is 0; that is, $T_{m\mathrm{fl}}=T_{m\mathrm{fr}}=0$.

When θ and φ are small, the vertical displacement of the join point of vehicle body and the four suspensions can be deduced:

$$
\begin{aligned}
z_1&=z_s-l_{\mathrm{f}}\theta+\frac{1}{2}d\varphi,\\
z_2&=z_s-l_{\mathrm{f}}\theta-\frac{1}{2}d\varphi,\\
z_3&=z_s+l_{\mathrm{r}}\theta+\frac{1}{2}d\varphi,\\
z_4&=z_s+l_{\mathrm{r}}\theta-\frac{1}{2}d\varphi.
\end{aligned}
\tag{2}
$$

The validity of the above dynamic equation has been verified in [12].

2.1.2. Tyre Model. The 16-degree-of-freedom rollover prediction model is a coupling dynamic model which considers

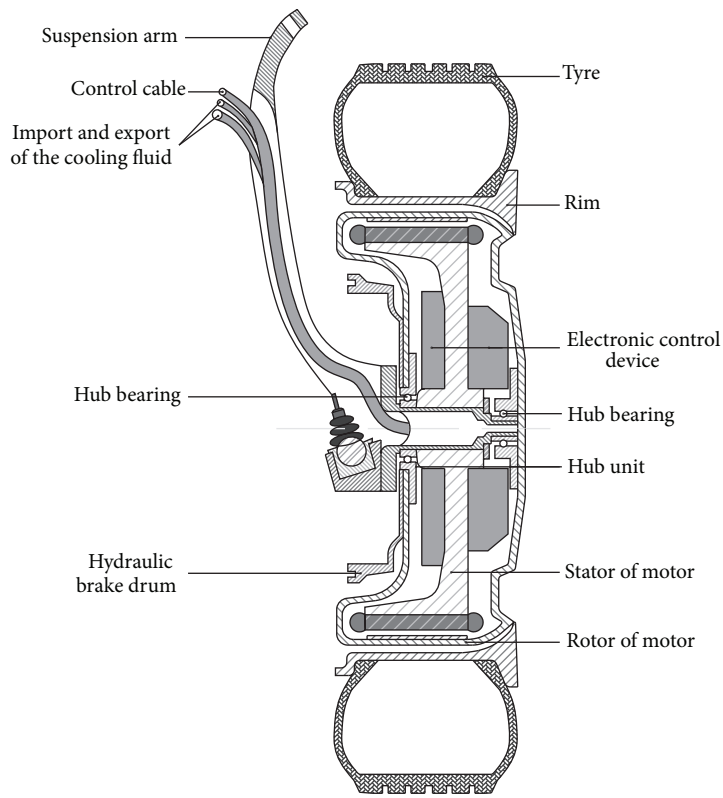

Figure 1: Basic structure of the IWM driven system.

the influence of vertical, lateral, and longitudinal dynamics on the vehicle rollover. Therefore, the Magic Formula Tyre Model proposed by Professor Pacejka is used to obtain the nonlinear tyre force accurately. The specific expression of the Magic Formula Tyre Model is [13]

$$y = D \sin \{C \arctan [Bx - E (Bx - \arctan Bx)]\}. \quad (3)$$

2.2. Input Model of Excitation Source

2.2.1. RSR Model of Four Wheels. For the rollover prediction model, four random RSR input signals are required for each wheel. Due to the mutual interference of the four-wheel RSR in the space domain, the RSR correlation between the four wheels is considered in the model. The state equation of the four-wheel RSR input model can be expressed as follows [14, 15]:

$$\dot{Z}(t) = AZ(t) + B_0 w(t), \quad (4)$$

where

$$Z(t) = [q_1(t) \;\; q_2(t) \;\; q_3(t) \;\; q_4(t) \;\; x_1(t) \;\; x_2(t)],$$

$$\dot{Z}(t) = [\dot{q}_1(t) \;\; \dot{q}_2(t) \;\; \dot{q}_3(t) \;\; \dot{q}_4(t) \;\; \dot{x}_1(t) \;\; \dot{x}_2(t)],$$

$$A = \begin{bmatrix} -2\pi n_c u & 0 & 0 & 0 & 0 & 0 \\ \frac{u}{B} e^{-2\pi n_c d} & -\frac{u}{d} & 0 & 0 & 0 & 0 \\ -12\frac{u}{l} - 2\pi n_c u & 0 & 0 & 0 & 0 & 1 \\ \frac{u}{B} e^{-2\pi n_c d} & -\left(12\frac{u}{l} + \frac{u}{d}\right) & 0 & 0 & 0 & 1 \\ -12\frac{u}{l} & 0 & 0 & 0 & 0 & 1 \\ 72\frac{u^2}{l^2} & 0 & 0 & 0 & -12\frac{u^2}{l^2} & -6\frac{u}{l} \end{bmatrix},$$

$$B_0 = [2\pi n_0 \sqrt{G_0 u} \;\; 0 \;\; 2\pi n_0 \sqrt{G_0 u} \;\; 0 \;\; 0 \;\; 0]. \quad (5)$$

Based on [16], the value of n_0 is $0.1\,\mathrm{m}^{-1}$, and n_c is $0.01\,\mathrm{m}^{-1}$ in this paper.

2.2.2. EMF Model. In this paper, the IWM is the permanent magnet synchronous motor. Ignoring the saturation effect and the core reluctance of the IWM powered by the sine-wave current, the flux density can be calculated as [17, 18]

$$B(\theta_t, t) = F(\theta_t, t)\,\Lambda(\theta_t, t). \quad (6)$$

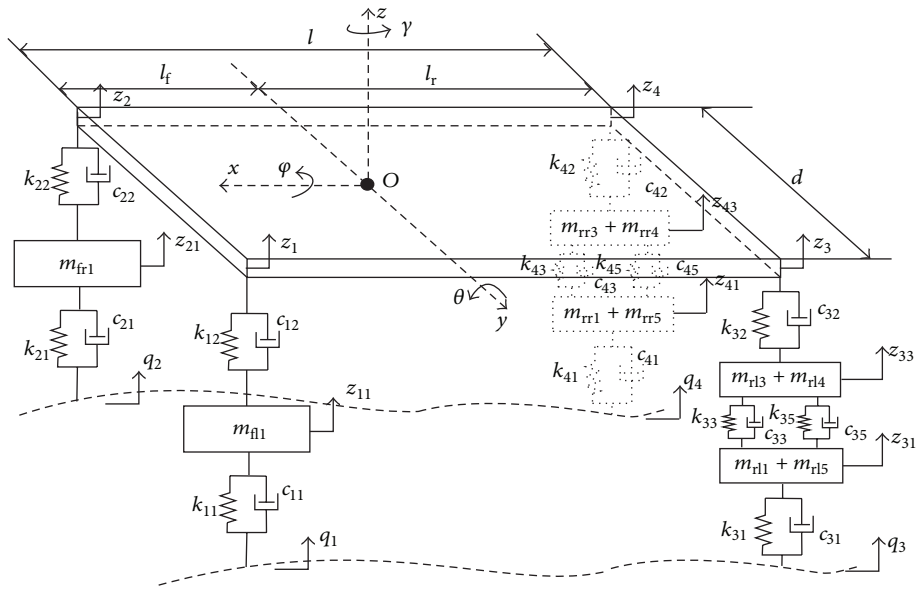

(a) Vertical dynamic model

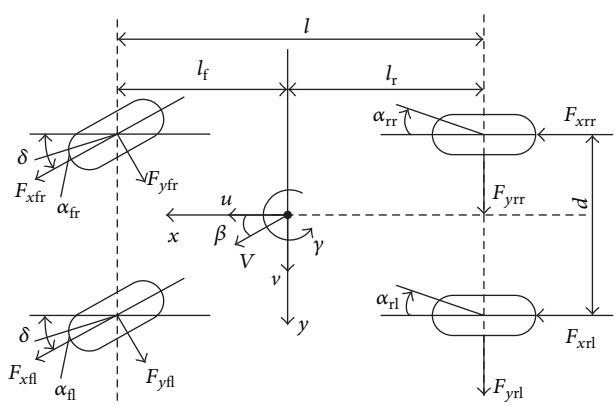

(b) Lateral dynamic model

Figure 2: Rollover prediction dynamic model.

(1) Magnet Gap Permeability Λ. For the ideal operating condition of the IWM, the geometric center of the rotor magnetic pole should coincide with that of the stator core. Additionally, the magnet gap length should be distributed along the circumference evenly. However, in reality the tyre runout under different RSR excitations and uneven load will cause the deformation in the IWM magnet gap, as shown in Figure 3.

The length of the even or uneven magnet gap of IWM as shown in Figure 3 at time t can be expressed as

$$g_e(\theta_t, z, t) = g_0(1 - \varepsilon(z)\cos(\theta_t - \omega_t t - \gamma_0)),$$
$$\varepsilon(z) = \frac{e}{g_0}. \tag{7}$$

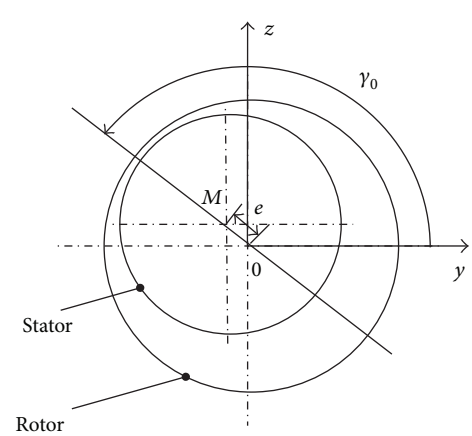

Figure 3: MGD of the IWM.

The Fourier series of the magnet gap permeance is calculated by

$$\Lambda(\theta_t, z, t) = \frac{\mu_0}{g_e(\theta_t, z, t)} = \sum_{\lambda=0}^{\infty} \Lambda_\lambda \cos[\lambda(\theta_t - \omega_t t - \gamma_0)], \tag{8}$$

where

$$\Lambda_\lambda = \begin{cases} \frac{\mu_0}{g_0}\Lambda'_0 = \frac{\mu_0}{g_0}\frac{1}{\sqrt{1-\varepsilon^2}} & \lambda = 0 \\ \frac{\mu_0}{g_0}\Lambda'_\lambda = 2\frac{\mu_0}{g_0}\frac{1}{\sqrt{1-\varepsilon^2}}\left(\frac{1-\sqrt{1-\varepsilon^2}}{\varepsilon}\right)^\lambda & \lambda \geq 1. \end{cases} \tag{9}$$

(2) Magnetomotive Force of the IWM. The magnetomotive force of the IWM is synthesized by the magnetomotive force of the permanent magnet and the stator winding, which can be expressed as

$$\begin{aligned} F(\theta, t) &= F_{s0}(\theta_t, t) + F_{s\nu}(\theta_t, t) + F_r(\theta_t, t) \\ &= F_0 \cos(\omega_t t - p\theta_t + \varphi_0) \\ &\quad + \sum_\nu F_\nu \cos(\omega_t t - \nu\theta_t + \varphi_\nu) \\ &\quad + \sum_\mu F_\mu \cos(\mu\omega_t t - \mu p\theta_t). \end{aligned} \tag{10}$$

(3) EMF Model. Substituting (8) and (10) into (6), the flux density is derived as

$$\begin{aligned} B(\theta_t, t) = &\Big[F_0 \cos(\omega_t t - p\theta_t + \varphi_0) \\ &+ \sum_\nu F_\nu \cos(\omega_t t - \nu\theta_t + \varphi_\nu) \\ &+ \sum_\mu F_\mu \cos(\mu\omega_t t - \mu p\theta_t)\Big] \\ &\cdot \left\{\frac{\mu_0}{g_0}\left[1 + \sum_{\lambda=1}^{\infty}\frac{\varepsilon^\lambda}{2^{\lambda-1}}\cos(\theta_t - \omega_t t - \gamma_0)\right]\right\}. \end{aligned} \tag{11}$$

Based on the Maxwell magnet stress tensor theory, the radial and tangential magnetic force density in a 2D magnetic field under polar coordinates can be calculated by [19, 20]

$$\begin{aligned} f_r &= \frac{1}{2\mu_0}\left(B_r^2 - B_t^2\right), \\ f_t &= \frac{1}{\mu_0}B_r B_t. \end{aligned} \tag{12}$$

Transforming the magnetic force from polar coordinate to Cartesian coordinate, the force acting on the stator and rotor in the z direction can be deduced by integrating the IWM axial gap length l_a as

$$\begin{aligned} F_z = l_a \int_0^{2\pi} (f_r \sin\alpha - f_t \cos\alpha) \cdot r d\alpha = \frac{r l_a}{2\mu_0} \\ \cdot \int_0^{2\pi} \left(\left(B_t(s,t)^2 - B_r(s,t)^2\right)\sin\alpha \right. \\ \left. - 2B_r(s,t) B_t(s,t)\cos\alpha\right) d\alpha. \end{aligned} \tag{13}$$

Table 1: Vehicle parameters.

Symbol	Unit	Value
m	kg	1450
m_s	kg	1160
I_x	kg·m^2	606
I_y	kg·m^2	1800
I_z	kg·m^2	2300
I_{xz}	kg·m^2	45
I_{wi}	kg·m^2	2.5
k_{j1} $(j = 1, 2, 3, 4)$	N/m	200000
c_{j1} $(j = 1, 2, 3, 4)$	N/(m/s)	100
k_{j2} $(j = 1, 2)$	N/m	35000
c_{j2} $(j = 1, 2)$	N/(m/s)	1500
k_{j2} $(j = 3, 4)$	N/m	40000
c_{j2} $(j = 3, 4)$	N/(m/s)	1800
$k_{33}, k_{43}, k_{35}, k_{45}$	N/m	8000000
l_f	m	1.2
l_r	m	1.4
d	m	1.44
h_s	m	0.488
r_t	m	0.3

2.2.3. Steering Input Model. The IWM driven EV used in this study is a front-wheel steering vehicle. The influence of the steering system on the wheel angle is ignored in the process of steering and the steering angle ratio is 15.

3. Rollover Characteristics of IWM Driven EV

3.1. Vehicle Parameters. The main vehicle parameters are listed in Table 1.

The IWM used in the vehicle is a surface-mount permanent magnet synchronous motor with an outer rotor and an inner stator. The slot and pole combination is 36-slot/12-pole type. The stator winding is a three-phase Y-type. The basic structure and detailed size of the IWM is shown in Figure 4.

3.2. Evaluation Index of Vehicle Rollover. When the vehicle rounds a curve, the greater the vehicle speed is, the greater the lateral acceleration is, but the vertical load of the inside wheels is reduced. In other words, the vertical load is transferred from the inside to outside. When the vertical load of the inside wheel is decreased to 0, the vehicle will not be able to maintain a balance in the roll plane and will begin to roll over.

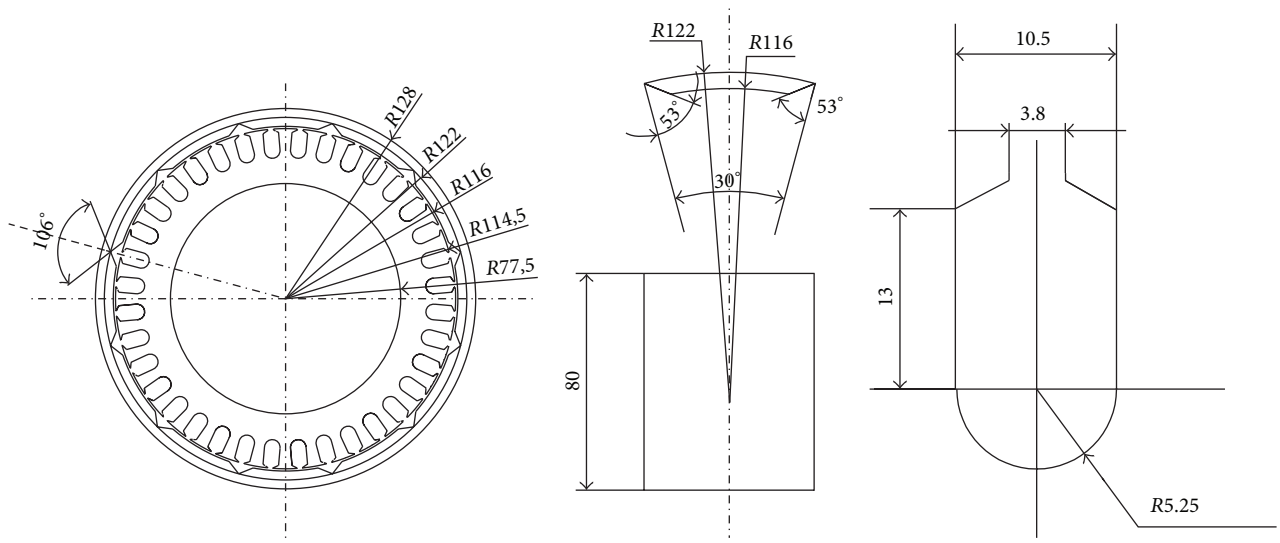

(a) Overall structure (b) Permanent magnet (c) Slot

Figure 4: Structure of the IWM.

This condition indicates that the vehicle is in an unstable state and that a rollover accident may easily occur. In light of this, a lateral load transfer rate (LTR) is selected as the evaluation index of the vehicle rollover stability. LTR is defined as the ratio of the transferred load from the inside wheel to the outside wheel and the total load [21, 22]; that is,

$$\mathrm{LTR} = \left| \frac{F_{\mathrm{zfl}} + F_{\mathrm{zrl}} - F_{\mathrm{zfr}} - F_{\mathrm{zrr}}}{F_{\mathrm{zfl}} + F_{\mathrm{zrl}} + F_{\mathrm{zfr}} + F_{\mathrm{zrr}}} \right|. \tag{14}$$

The vertical load of the four wheels can be calculated by

$$\begin{aligned} F_{\mathrm{zfl}} &= \frac{mgl_{\mathrm{r}}}{2l} - ma_x' \frac{h}{2l} - \frac{ma_y' h l_{\mathrm{r}}}{dl} - \frac{K_{\mathrm{f}}\varphi + C_{\mathrm{f}}\dot{\varphi}}{d} \\ F_{\mathrm{zfr}} &= \frac{mgl_{\mathrm{r}}}{2l} - ma_x' \frac{h}{2l} + \frac{ma_y' h l_{\mathrm{r}}}{dl} + \frac{K_{\mathrm{f}}\varphi + C_{\mathrm{f}}\dot{\varphi}}{d} \\ F_{\mathrm{zrl}} &= \frac{mgl_{\mathrm{f}}}{2l} + ma_x' \frac{h}{2l} - \frac{ma_y' h l_{\mathrm{f}}}{dl} - \frac{K_{\mathrm{r}}\varphi + C_{\mathrm{r}}\dot{\varphi}}{d} \\ F_{\mathrm{zrr}} &= \frac{mgl_{\mathrm{f}}}{2l} + ma_x' \frac{h}{2l} + \frac{ma_y' h l_{\mathrm{f}}}{dl} + \frac{K_{\mathrm{r}}\varphi + C_{\mathrm{r}}\dot{\varphi}}{d}, \end{aligned} \tag{15}$$

where

$$\begin{aligned} a_x' &= a_x - \frac{m_s h_s \ddot{\theta}}{m}, \\ a_y' &= a_y + \frac{m_s h_s \ddot{\varphi}}{m}. \end{aligned} \tag{16}$$

When the vehicle moves in a straight line on the flat and level road, the vertical load of the wheels on both sides is approximately equal, and LTR is close to 0. When the vehicle rounds a curve or the roll angle is unduly large, LTR increases; as LTR is increased to 1, the inside wheel leaves the ground and the vertical load is 0, at which point a rollover accident may likely occur.

3.3. Simulation Test and Results Analysis

3.3.1. Simulation Test Conditions. As a typical test condition, FTF steering can be well used to examine the vehicle rollover stability in an extreme manipulation condition such as quick steering wheel correction and opposite rotation [23]. Therefore, the FTF test is considered as the steering maneuver test condition.

To set the FTF test condition, a steering wheel reference value $\Delta\delta$ is determined. Based on [24], the reference value $\Delta\delta$ is 25°. Then, the FTF condition can be set with $\Delta\delta$, as shown in Figure 5. Under the full load condition, the vehicle moves in a straight line at 80 km/h until it reaches a steady state; the driver quickly turns the steering wheel at the speed of 720°/s. Then, when the steering wheel reaches the maximum steering value δ_0 ($\delta_0 = 6.5 \times \Delta\delta$), the driver keeps it for 250 ms and then rotates the steering wheel in the opposite direction with the same speed. As the steering wheel reaches $-\delta_0$, the driver keeps it for 3 s, after which the driver returns the steering wheel to the original position quickly.

Grade B RSR input is calculated using (4), where the vehicle speed u is still kept at 80 km/h.

3.3.2. Contrastive Analysis of the Results. The above FTF steering condition and RSR input are substituted into the mathematical model of vehicle rollover to calculate the vertical load of the wheels with or without EMF. The change in vertical load of the four wheels is obtained, as shown in Figure 6. Then, LTR can be calculated using (14), as shown in Figure 7.

Because vehicle rollover is a very complex transient process, rollover will occur whenever the LTR is too large. Therefore, the peak value of the transient LTR plays an important role in the evaluation of vehicle rollover risk. Statistical analysis is carried out for the above results to understand the effect of EMF on the response variables more

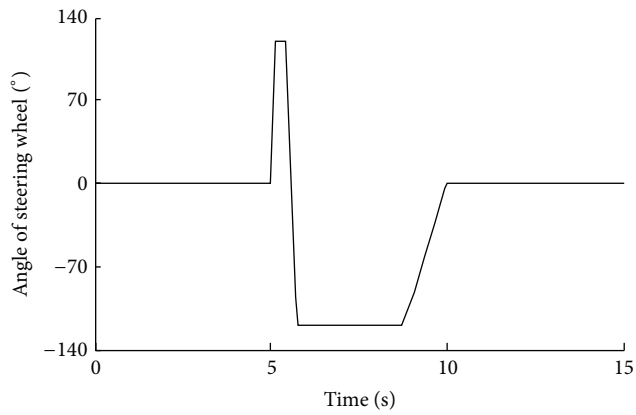

Figure 5: Input of the steering wheel.

Table 2: Statistical analysis of the response variables.

		With EMF	Without EMF	Rate of change
F_{zfl} (N)	Maximum	6455	6327	2.02%
	Minimum	1528	1635	6.54%
F_{zfr} (N)	Maximum	6166	6053	1.87%
	Minimum	1202	1328	9.49%
F_{zrl} (N)	Maximum	6152	5431	13.28%
	Minimum	620	1365	54.58%
F_{zrr} (N)	Maximum	5857	5159	13.53%
	Minimum	467	1124	58.45%
LTR	Maximum	0.7184	0.6341	13.29%

clearly. The maximum, minimum, and change rate for each response variable are listed in Table 2.

According to the comparison results shown in Figures 6 and 7 and Table 2, we can see the condition in which the load transfer of four wheels occurs and the impact on the vertical load of the wheels due to the EMF caused by the RSR is revealed. In particular, this effect can be seen upon the two rear drive wheels, because the EMF generated by the drive motors acts on the corresponding stator and rotor directly and transmits to the rear wheels. With the influence of EMF, the maximum and minimum change rates in vertical load of the left rear wheel are 13.28% and 54.58%, respectively, while that of the change rate without the influence of EMF in vertical load of the left rear wheel can reach 13.53% and 58.45%. Comparison results of the LTR show that LTR has larger fluctuation across the whole simulation test due to the influence of EMF. Additionally, the peak value of LTR is increased from 0.6341 to 0.7184, a relative increase of 13.29% after the consideration of EMF. This indicates that the EMF has some effect on the vertical load transfer and reduces the antirollover ability of the vehicle.

The EMF generated by the two rear IWMs in the simulation test is shown in Figure 8.

As seen from Figure 8, the EMF generated by the left and right IWMs is different and the EMF is increased when the steering wheel is rotated quickly. The reason for this effect lies in the difference of the left and right RSR input and the vertical load transfer under the steering condition, which makes the magnet gap have a different deformation and generates a different amount of EMF. As shown in the figure, the EMF maximum generated by the left rear IWM can reach 1012 N, while the EMF maximum generated by the right rear IWM is 928 N.

3.4. Analysis of Road-Influenced Factor. Firstly, the EMF is caused by the road excitation, and different road conditions lead to the generation of different amounts of EMF which will influence the vehicle rollover in varying degrees. Therefore, it is necessary to further study the influence of different road conditions on vehicle rollover. For the RSR input, road level and vehicle speed are two important factors, while the adhesive coefficient is significant for the vehicle steering stability. So, the analysis of road level, vehicle speed, and road adhesion coefficient on the vehicle rollover is carried out in this section.

In the further study, only one influenced factor is changed, whereas the rollover dynamic model, excitation input, and simulation condition are all the same.

3.4.1. Factor of Road Level. Road level is set as grades A, B, and C. That is, the road roughness coefficient is 16×10^{-6}, 64×10^{-6}, and 256×10^{-6} m^3, respectively. A larger road roughness coefficient corresponds to a lager RSR excitation. Then the LTR of different road levels can be obtained, as shown in Figure 9. Vehicle speed is kept at 80 km/h in the simulation.

As shown in Figure 9, the value of LTR increases with the increase of the road roughness coefficient. That is, the rollover stability deteriorates with the increase of road level and LTR expresses larger fluctuation when the road roughness coefficient is larger.

Statistical analysis of the simulation results is carried out and the relation of the road level and the peak value of LTR and EMF are obtained, as shown in Figures 10 and 11.

As seen from Figure 10, the road level has an effect on the peak value of LTR with a near-linear increasing trend. Additionally, the change rate of LTR can reach 7.34% when the road level is increased from grade A to C. The reason for this effect is that the worse road level makes the RSR excitation increase. The increase in RSR excitation not only causes larger vertical load transfer under the steering condition but further exacerbates the IWM MGD which produces larger EMF and has a certain impact on the LTR. From Figure 11, we can see that the IWM EMF increases with the increase of road level, which further confirms the illustration for the results above.

3.4.2. Factor of Vehicle Speed. In this section, the road adhesion coefficient is 0.6. Vehicle speed is set as 40, 80, and 120 km/h; that is, the rotating speed of IWM is 354, 707, and 1061 rpm. A higher vehicle speed means larger RSR excitation according to (4). Accordingly, the LTR of different vehicle speeds under the grade B FTF condition can be obtained, as shown in Figure 12.

As shown in Figure 12, the LTR increases with the increase of vehicle speed. When the vehicle speed is 120 km/h, the maximum of LTR can reach up to 0.7577, and the LTR still

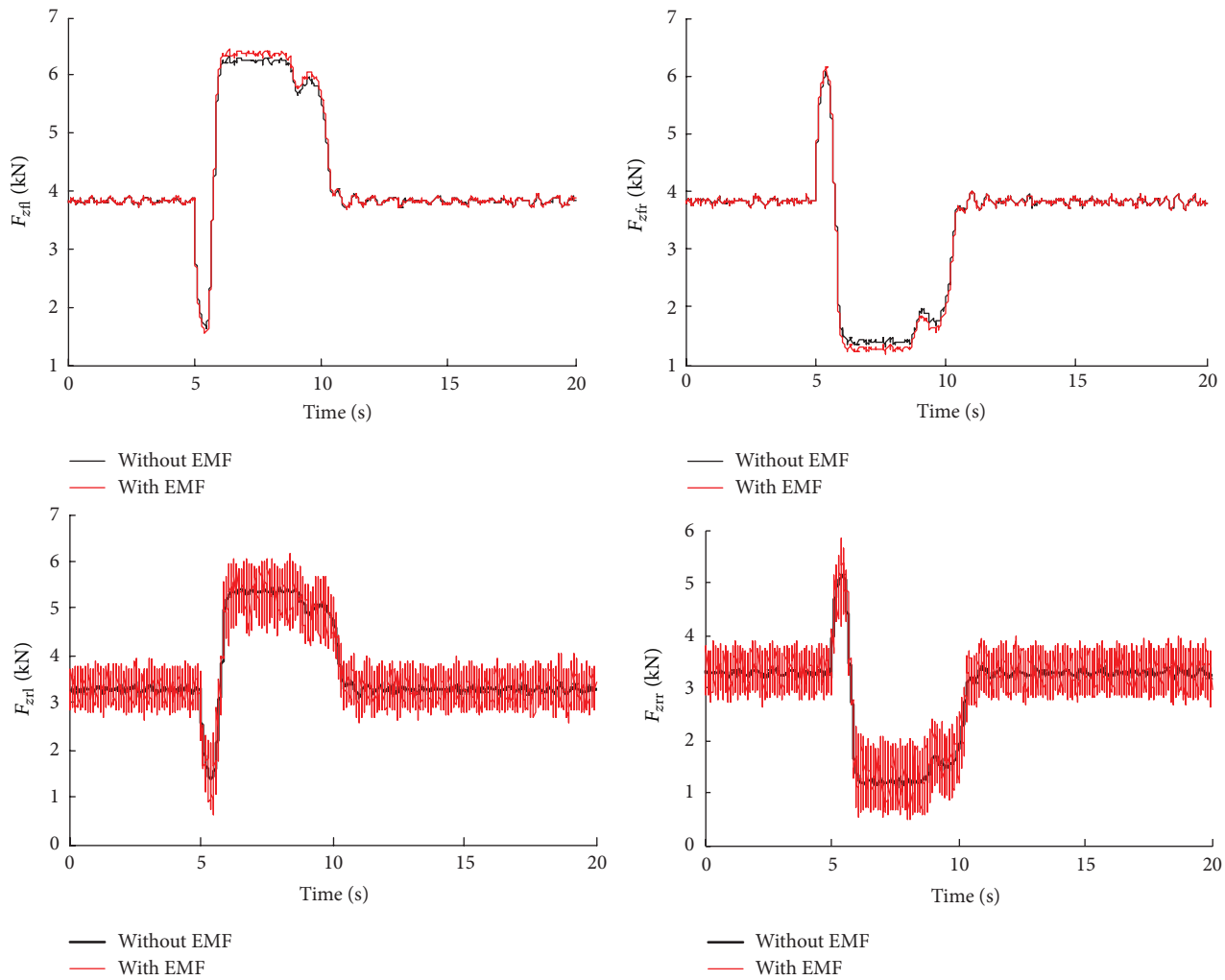

Figure 6: Vertical load of the four wheels.

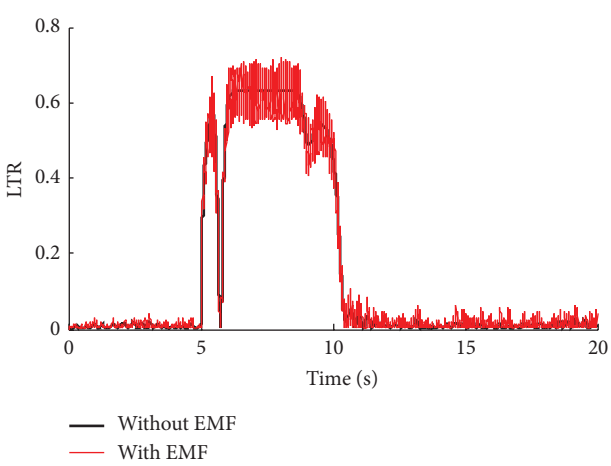

Figure 7: Comparison result of the vehicle LTR with/without EMF.

remains at a higher level even if the steering wheel has been returned to its original position at 10 s. The results indicate that the recovery capability of the straight line driving is decreased with the increase of the vehicle speed in the course of turning. For a certain road level, the available traction is a constant value under the same sideslip angle. When the vehicle speed is increased, larger traction is needed to meet the demand for the longitudinal driving resistance. Therefore, if the vehicle speed reaches a certain level, it is likely that vehicle slide will take place because the smaller amount of traction is not sufficient to meet the demand for the lateral forces and the vehicle will be unable to drive according to a predetermined path.

Similarly, statistical analysis of the simulation results is carried out, and the relation of vehicle speed to the peak value of LTR and EMF is obtained, as shown in Figures 13 and 14.

As shown in Figures 13 and 14, the peak value of LTR is increased obviously with the increase of vehicle speed. This is due to the increased vehicle speed which causes the increase of the RSR excitation. The increase in RSR excitation not only influences the size of LTR but further exacerbates the IWM MGD which will produce bigger EMF and have a certain impact on LTR. According to the data of Figure 13, the growth rate of LTR can reach 29.91% when the vehicle speed is

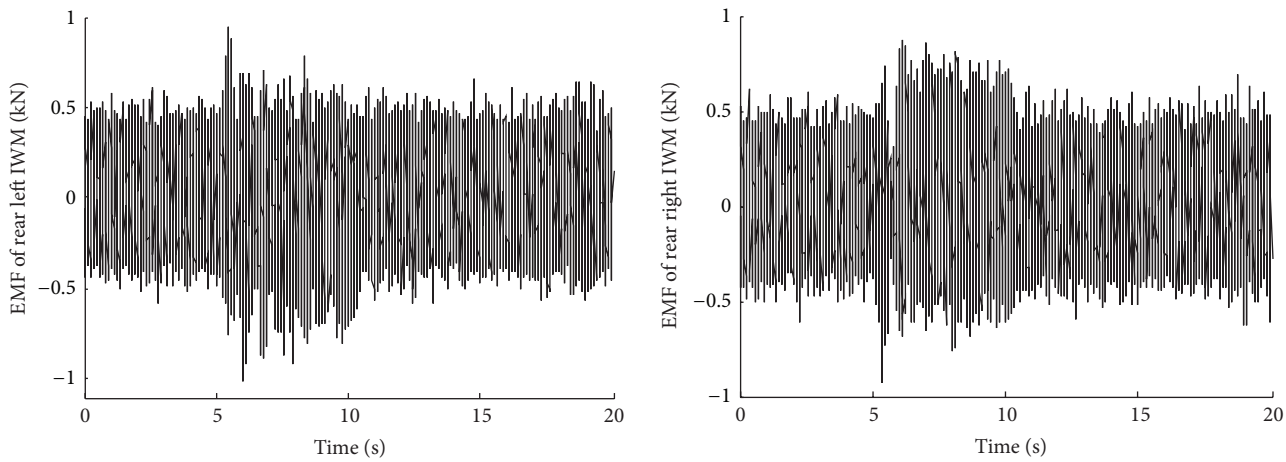

Figure 8: EMF of the IWMs.

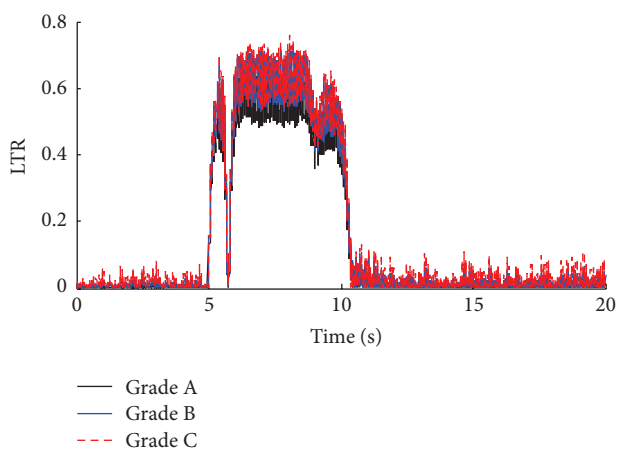

Figure 9: LTR in different road level.

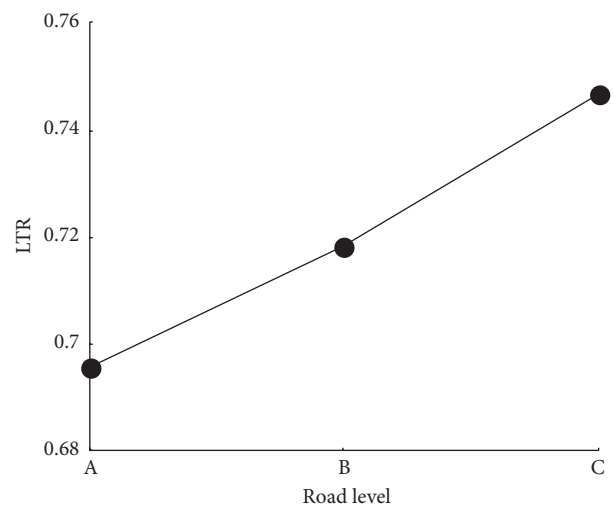

Figure 10: Relation of the road level and peak value of LTR.

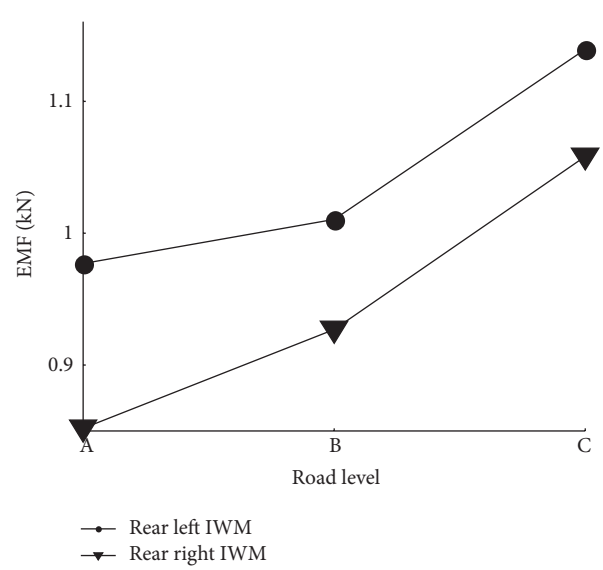

Figure 11: Relation of the road level and peak value of EMF.

increased from 40 to 80 km/h, while the growth rate of LTR is 5.47% as the vehicle speed is increased from 80 to 120 km/h. It follows that the LTR is influenced strongly in the low vehicle speed range. In contrast, there is a slight influence on the LTR in the high speed range.

3.4.3. Factor of Road Adhesion Coefficient. Vehicle speed is kept at 80 km/h, and the road adhesion coefficient is set as 0.3, 0.6, and 0.9. Afterwards, the LTR can be obtained with different adhesion coefficients under the B level FTF steering condition, as shown in Figure 15.

As shown in Figure 15, the rollover risk (LTR value) of the vehicle is increased with the increase of the road adhesion coefficient. This condition indicates that a lower value of road adhesion coefficient is better for the vehicle rollover safety. However, the result also shows that the lower the road adhesion coefficient is, the worse the vehicles follow the predetermined winding roads. As seen from the figure, when the adhesion coefficient is 0.3, the LTR value always maintains the state before the steering wheel reset and cannot return to the straight line driving even if the steering wheel has been

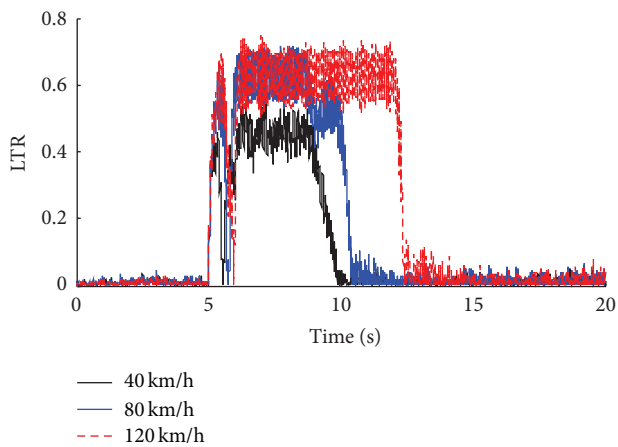

Figure 12: LTR in different vehicle speed.

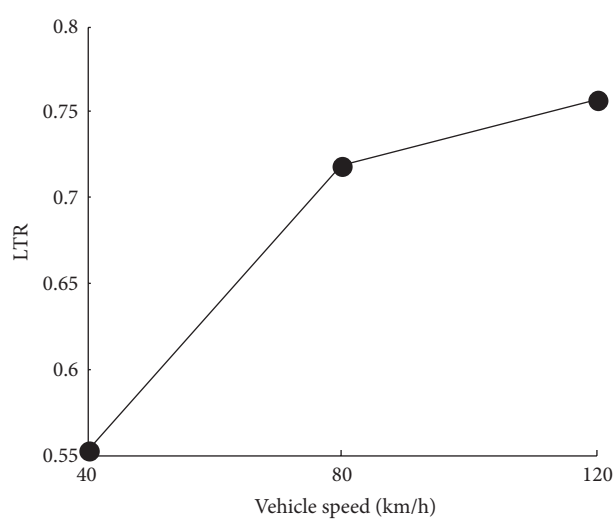

Figure 13: Relation of the vehicle speed and peak value of LTR.

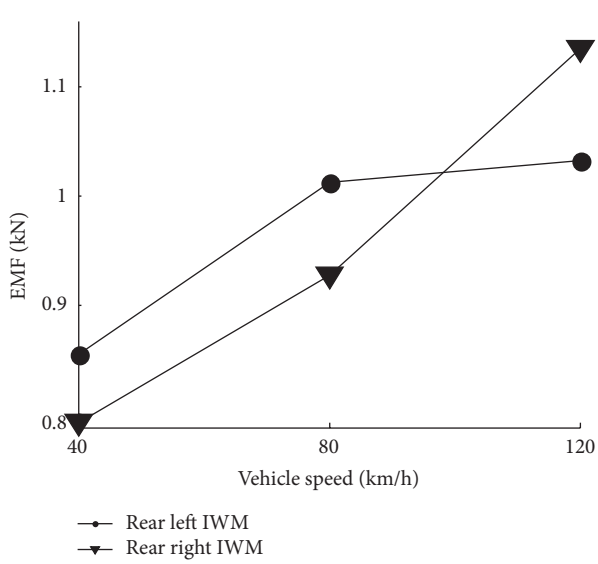

Figure 14: Relation of the vehicle speed and peak value of EMF.

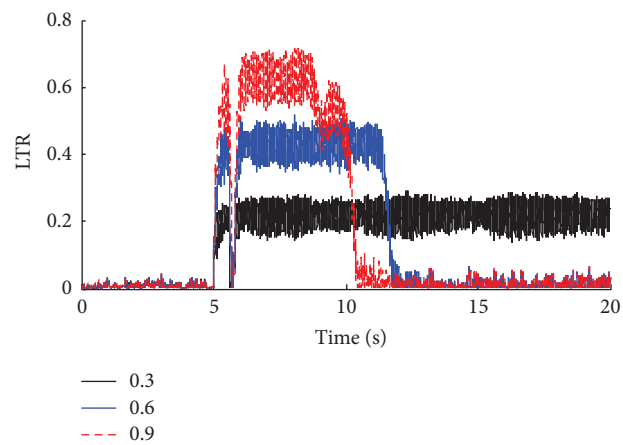

Figure 15: LTR in different road adhesion coefficient.

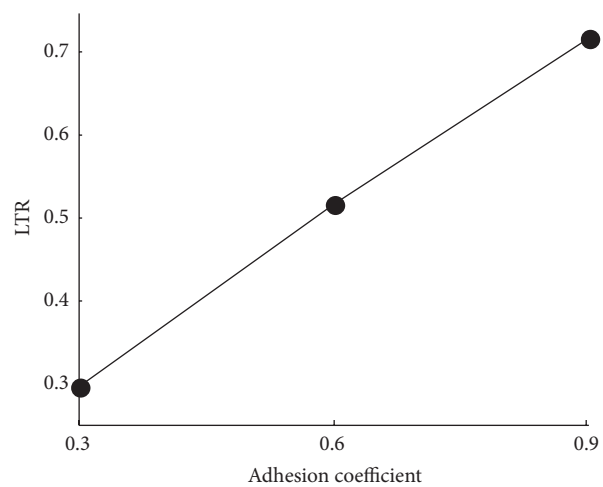

Figure 16: Relation of the adhesion coefficient and peak value of LTR.

returned to its original position at 10 s. This is because low amounts of traction can only be provided by the road with a lower adhesion coefficient, which is not sufficient to meet the demand for the lateral forces of the vehicle during the rapid turning condition. Although vehicle rollover caused by the curvilinear motion is less likely on a low adhesion road, slippage can easily occur. However, if there are obstacles on the road, it is highly likely that a rollover will occur due to the lateral impact of the vehicle and the obstacles.

The relation of adhesion cohesion to the peak value of LTR and EMF is obtained based on statistical analysis, as shown in Figures 16 and 17.

As shown in Figure 16, the peak value of LTR is increased linearly with the increase of the vehicle speed. When the adhesion coefficient is increased from 0.3 to 0.9, the corresponding peak value of LTR is increased from 0.2947 to 0.718, and the growth rate of LTR can reach 143.77%. As shown in Figure 17, the road adhesion coefficient also has a great influence on the IWM EMF and a larger adhesion coefficient makes the EMF increase.

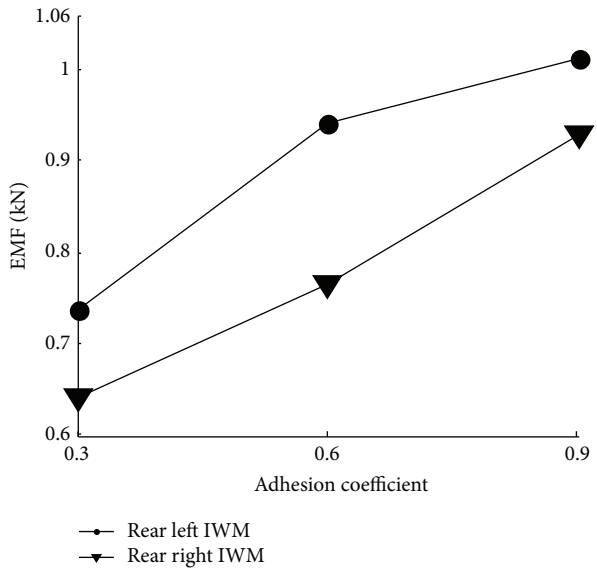

Figure 17: Relation of the adhesion coefficient and peak value of EMF.

4. Discussion and Conclusions

In this paper, a verified 16-degree-of-freedom rollover dynamic model is introduced to study the rollover stability of the IWM driven EVs. Vehicle rollover characteristic with or without EMF under the grade B and FTF steering condition is analyzed. In addition, further study is carried out to understand the vehicle rollover in different road level, vehicle speed, and road adhesion coefficient. Based on this study, some conclusions can be obtained:

(1) Comparative analysis of the vehicle rollover with and without EMF shows the following: ① The EMF caused by the RSR has a certain impact on the vertical load transfer of the wheels, especially for the drive wheels. ② The LTR has a larger fluctuation across the whole simulation test due to the influence of EMF. Additionally, the EMF makes the LTR increase, which indicates that the EMF has some effect on the vertical load transfer, and reduces the antirollover ability of the vehicle. Therefore, the effect of IWM EMF on the vehicle rollover should be considered in the design of the IWM driven EV. ③ The size of the EMF is related to the RSR and steering input condition after the type and the structure of the electric wheel system are determined. The reason lies in the difference of the left and right RSR input and the vertical load transfer under the steering condition, which makes the magnet gap have different deformation and, therefore, cause different size of EMF.

(2) Further study of the effect of the road-influenced factors on the vehicle rollover shows that the fluctuation and peak value of the LTR increase with an increase of the road level, vehicle speed, and road adhesion coefficient. That is, the vehicle rollover stability is worse with the increase of the above factors. The reason is that poor road conditions not only cause larger vertical load transfer but further exacerbate the IWM MGD which produces bigger EMF and impacts the load redistribution.

(3) For the three road-influenced factors, road adhesion coefficient has the greatest effects on the vehicle rollover, followed by the vehicle speed and road level. From the vehicle rollover safety perspective, the road adhesion coefficient should be small. However, if the adhesion coefficient is too small, traction is diminished. Therefore, vehicle slippage will occur because the smaller traction is not sufficient to keep the vehicle running stability. As a result, the road adhesion coefficient should be considered in the design of the vehicle. For the vehicle speed, the recovery capability of straight line driving decreases with the increase of the vehicle speed in the course of turning. If the vehicle speed reaches a certain level, it is likely that vehicle slippage will take place and the vehicle will be unable to drive according to the predetermined path. So, the vehicle speed should be decreased to keep the vehicle stable. Although there is little effect on vehicle rollover by the road lever relative to other factors, it also needs to be considered to improve the vehicle rollover stability in the design.

This paper provides certain theory basis for the design of the IWM driven EVs.

Appendix

Notations

u:	Longitudinal speed of vehicle
v:	Lateral speed of vehicle
a_y:	Lateral acceleration of vehicle
δ:	Angle of the front wheels
γ:	Yaw rate of the vehicle
φ:	Pitch angle of the vehicle body
θ:	Roll angle of the vehicle body
l:	Wheel base
fl, fr, rl, rr:	Front left, front right, rear left, and rear right wheel of the vehicle
l_f, l_r:	Distance of mass center to the front and rear axle
d:	Wheel track
h_s:	Distance of the body mass center to roll center axis
F_{xi}:	Longitudinal force of the wheel, i = fl, fr, rl, rr
F_{yi}:	Cornering force of the wheel, i = fl, fr, rl, rr
α_i:	Slip angle of the wheel, i = fl, fr, rl, rr
m_{i1}:	Mass of tyre of the rear wheel, i = rl, rr

m_{i3}: Mass of the supporting shaft and brake caliper of the rear wheel, $i = \mathrm{rl}, \mathrm{rr}$
m_{i4}: Mass of the IWM stator and housing of the rear wheel, $i = \mathrm{rl}, \mathrm{rr}$
m_{i5}: Mass of the IWM rotor and brake disc of the rear wheel, $i = \mathrm{rl}, \mathrm{rr}$
k_{j1}, k_{j2}: Stiffness of the tyre and suspension, $j = 1, 2, 3, 4$
c_{j1}, c_{j2}: Damping of the tyre and suspension, $j = 1, 2, 3, 4$
q_j: Road surface roughness excitation, $j = 1, 2, 3, 4$
$k_{33}, k_{43}, k_{35}, k_{45}$: Stiffness of the bearing
$c_{33}, c_{43}, c_{35}, c_{45}$: Damping of the bearing
$z_{11}, z_{21}, z_{31}, z_{33}, z_{41}, z_{43}$: Vertical displacement of the corresponding mass
z_s: Vertical displacement of the vehicle body
z_j: Vertical displacement of the join point of vehicle body and the four suspensions, $j = 1, 2, 3, 4$
m: Mass of the vehicle
m_s: Mass of the vehicle body
I_{xz}: Inertia product of roll and yaw motion
I_x: Roll moment of inertia of vehicle body about x-axis
I_y: Pitch moment of inertia of vehicle body about y-axis
I_z: Yaw moment of inertia of vehicle about z-axis
T_{mi}: Torque of the in-wheel motor, $i = \mathrm{rl}, \mathrm{rr}$
I_{wi}: Moment of inertia of the wheel, $i = \mathrm{fl}, \mathrm{fr}, \mathrm{rl}, \mathrm{rr}$
w_i: Rotated speed of the wheel, $i = \mathrm{fl}, \mathrm{fr}, \mathrm{rl}, \mathrm{rr}$
r_t: Wheel radius
G_0: Coefficient of the road surface roughness
n_0: Reference spatial frequency
B: Stiffness coefficient of the tyre
C: Shape factor of the tyre characteristic curve
D: Peak value of the tyre characteristic curve
E: Control factor for the curvature at the peak of the tyre characteristic curve
n_c: Low cutoff frequency
F: Total magnetomotive force
Λ: Magnet gap permeance
g_e: Magnet gap length in circumference
g_0: Nominal gap thickness
e: Relative displacement between stator and rotor
ε: Magnet gap eccentricity
ω_t: Rotated speed of the motor
θ_t: Initial position angle between the stator and rotor
μ_0: Vacuum permeability
Λ_λ: Fourier coefficient
Λ: Fourier series
F_{s0}, F_{sv}: Fundamental and v order magnetomotive force of stator winding
F_r: Magnetomotive force of permanent magnet
F_0, F_v: Amplitude of the fundamental and v order magnetomotive force of stator winding
F_μ: Amplitude of the μ order magnetomotive force of permanent magnet
p: Number of pole pairs
B_r, B_t: Magnetic flux densities in radial and tangential direction
l_a: Axial gap length of the motor
r: Integral radius
F_{zi}: Vertical load of the wheels, $i = \mathrm{fl}, \mathrm{fr}, \mathrm{rl}, \mathrm{rr}$
h: Height of vehicle mass center
$K_\mathrm{f}, K_\mathrm{r}$: Rolling angular stiffness of the front and rear axle
$C_\mathrm{f}, C_\mathrm{r}$: Rolling angular damping of the front and rear axle.

Abbreviations

EV: Electric vehicle
EMF: Electromagnetic force
FTF: Fixed Timing Fishhook
IWM: In-wheel motor
LTR: Load transfer rate
MGD: Magnet gap deformation
RSR: Road surface roughness.

Competing Interests

The authors declare that they have no competing interests.

Acknowledgments

This research is supported by the National Natural Science Foundation of China (Grant no. 51405273) and sponsored by Shandong Province Higher Educational Science and Technology Program (Grant no. J14LB08) and Young Teachers Development Support Program for Shandong University of Technology.

References

[1] National Highway Traffic Safety Administration, *An Analysis of Motor Vehicle Rollover Crashes and Injury Outcomes*, NHTSA, Washington, DC, USA, 2007.
[2] J. J. Xia, L. Chang, X. M. Hu et al., "Active control on the side tumbling of heavy vehicle based on model forecast,"

Transactions of the Chinese Society of Agricultural Engineering, vol. 26, no. 9, pp. 176–180, 2010.

[3] R. Kamnik, F. Boettiger, and K. Hunt, "Roll dynamics and lateral load transfer estimation in articulated heavy freight vehicles," *Proceedings of the Institution of Mechanical Engineers Part D: Journal of Automobile Engineering*, vol. 217, no. 11, pp. 985–997, 2003.

[4] Y. I. Ryu, D. O. Kang, S. J. Heo, and J. H. In, "Rollover mitigation for a heavy commercial vehicle," *International Journal of Automotive Technology*, vol. 11, no. 2, pp. 283–287, 2010.

[5] H. Imine, A. Benallegue, T. Madani, and S. Srairi, "Rollover risk prediction of heavy vehicle using high-order sliding-mode observer: experimental results," *IEEE Transactions on Vehicular Technology*, vol. 63, no. 6, pp. 2533–2543, 2014.

[6] H. Imine, L. M. Fridman, and T. Madani, "Steering control for rollover avoidance of heavy vehicles," *IEEE Transactions on Vehicular Technology*, vol. 61, no. 8, pp. 3499–3509, 2012.

[7] X. W. Song, J. Li, and Y. Wang, "A refined vehicle rollover model and its application," *Automotive Engineering*, vol. 31, no. 10, pp. 971–974, 2009.

[8] W. N. Bao and S. B. Hu, "Vehicle rollover simulation analysis considering road excitation," *Transactions of the Chinese Society of Agricultural Engineering*, vol. 31, no. 2, pp. 59–65, 2015.

[9] G. Nagaya, "*In-wheel Motor System*," US Patent, Patent No. US7287611 B2, 2007.

[10] A. Watts, A. Valance, A. Whitehead et al., "The technology and economics of in-wheel-motors," SAE 2010-01-2307, SAE International, 2010.

[11] Y. T. Luo and D. Tan, "Study on the dynamics of the in-wheel motor system," *IEEE Transactions on Vehicular Technology*, vol. 61, no. 8, pp. 3510–3518, 2012.

[12] C. Lu, D. Tan, and X. Y. Gang, "Parameter sensitivity analysis of coupling dynamics of in-wheel motor driving electric vehicle," *Science Technology and Engineering*, vol. 15, no. 28, pp. 78–87, 2015.

[13] H. B. Pacejka, *Tyre and Vehicle Dynamics*, Butterworth Heinemann, Oxford, UK, 2002.

[14] L. J. Zhang and T. X. Zhang, "Study on general model of random inputs of the vehicle with four wheels correlated in time domain," *Journal of Agricultural Machinery Engineering*, vol. 36, no. 12, pp. 29–31, 2005.

[15] L. J. Zhang, *Random Vibration of Vehicle*, Northeastern University Press, Shenyang, China, 2007.

[16] F. Yu and Y. Lin, *Vehicle System Dynamics*, China Machine Press, Beijing, China, 2005.

[17] A. M. El-Refaie, T. M. Jahns, and D. W. Novotny, "Analysis of surface permanent magnet machines with fractional-slot concentrated windings," *IEEE Transactions on Energy Conversion*, vol. 21, no. 1, pp. 34–43, 2006.

[18] J. Wang, Z. P. Xia, S. A. Long, and D. Howe, "Radial force density and vibration characteristics of modular permanent magnet brushless AC machine," *IEE Proceedings: Electric Power Applications*, vol. 153, no. 6, pp. 793–801, 2006.

[19] K. F. Rasmussen, "Analytical prediction of magnetic field from surface mounted permanent magnet motor," in *Proceedings of the IEEE International Electric Machines and Drives Conference (IEMDC '99)*, pp. 34–36, Seattle,. Wash, USA, May 1999.

[20] Z. Q. Zhu, D. Howe, and C. C. Chan, "Improved analytical model for predicting the magnetic field distribution in brushless permanent-magnet machines," *IEEE Transactions on Magnetics*, vol. 38, no. 1, pp. 229–238, 2002.

[21] Y. H. Lee and S. J. Yi, "Rollover prevention for sport utility vehicle using fuzzy logic controller," in *ICMIT 2005: Control Systems and Robotics*, vol. 6042 of *Proceedings of SPIE*, pp. 1–6, The International Society for Optical Engineering, Chongqing, China, September 2005.

[22] Y. Kim, G. Kim, and J. Lim, "Sensitivity analysis of commercial vehicle parameters on dynamic rollover," in *Proceedings of the 13th IPC on Automotive Engineering*, pp. 51–62, Gyeongju, Republic of Korea, 2005.

[23] H. Aleksander, B. Todd, and M. John, "Detection of vehicle rollover,," SAE 2004-01-1757, 2004.

[24] G. J. Forkenbrock and W. R. Grrott, "An experimental examination of J-turn and Fish-hook maneuvers that may induce on road, untripped light vehicle roller," SAE 2003-01-1008, 2003.